Biochimica et Biophysica Acta 1850 (2015) 1297–1309

Contents lists available at ScienceDirect

Biochimica et Biophysica Acta

journal homepage: www.elsevier.com/locate/bbagen

The role of His-83 of yeast apurinic/apyrimidinic endonuclease Apn1 in catalytic incision of abasic sites in DNA

Elena S. Dyakonova [a], Vladimir V. Koval [a,b], Alexander A. Lomzov [a,b], Alexander A. Ishchenko [c], Olga S. Fedorova [a,b,*]

[a] Institute of Chemical Biology and Fundamental Medicine, Siberian Branch of the Russian Academy of Sciences, Lavrentyev Ave., 8, Novosibirsk, 630090, Russian Federation
[b] Novosibirsk State University, Pirogov St., 2, Novosibirsk, 630090, Russian Federation
[c] Groupe «Réparation de l'ADN», Université Paris-Sud XI, UMR8200 CNRS, Institut Gustave Roussy, Villejuif Cedex F-94805, France

ARTICLE INFO

Article history:
Received 9 October 2014
Received in revised form 16 February 2015
Accepted 4 March 2015
Available online 10 March 2015

Keywords:
AP endonuclease
Abasic site
DNA repair
Base excision repair
2-Aminopurine
MD simulation

ABSTRACT

Background: The apurinic/apyrimidinic (AP) endonuclease Apn1 from *Saccharomyces cerevisiae* is a key enzyme involved in the base excision repair (BER) at the cleavage stage of abasic sites (AP sites) in DNA. The crystal structure of Apn1 from *S. cerevisiae* is unresolved. Based on its high amino acid homology to *Escherichia coli* Endo IV, His-83 is believed to coordinate one of three Zn^{2+} ions in Apn1's active site similar to His-69 in Endo IV. Substituting His-83 with Ala is proposed to decrease the AP endonuclease activity of Apn1 owing to weak coordination of Zn^{2+} ions involved in enzymatic catalysis.
Methods: The kinetics of recognition, binding, and incision of DNA substrates with the H83A Apn1 mutant was investigated. The stopped-flow method detecting fluorescence intensity changes of 2-aminopurine (2-aPu) was used to monitor the conformational dynamics of DNA at pre-steady-state conditions.
Results: We found substituting His-83 with Ala influenced catalytic complex formation and further incision of the damaged DNA strand. The H83A Apn1 catalysis depends not only on the location of the mismatch relative to the abasic site in DNA, but also on the nature of damage.
Conclusions: We consider His-83 properly coordinates the active site Zn^{2+} ion playing a crucial role in catalytic incision stage. Our data prove suppressed enzymatic activity of H83A Apn1 results from the reduced number of active site Zn^{2+} ions.
General significance: Our study provides insights into mechanistic specialty of AP site repair by yeast AP endonuclease Apn1 of Endo IV family, which members are not found in mammals, but are present in many microorganisms. The results will provide useful guidelines for design of new anti-fungal and anti-malarial agents.

1. Introduction

Apurinic/apyrimidinic (AP) endonucleases are divided in two families based on sequence identity to *Escherichia coli* enzymes Exo III and Endo IV. Members of Exo III family are found in all kingdoms of living organisms, whereas the Endo IV ones are more common in lower organisms, but are absent in plants, insects, mammals, and some vertebrates [1].

Yeast AP endonuclease Apn1 from *Saccharomyces cerevisiae* is a 41.4 kDa monomeric protein consisting of 367 amino acids with a theoretical pI = 8.43 [2–5]. It shares 42% amino acid sequence identity with *E. coli* Endo IV over regions encompassing 95% of the bacterial protein and 285 amino acids of the N-terminus of the yeast protein (Fig. 1) [6]. Apn1's C-terminus consists of 82 amino acid residues including two Lys/Arg clusters, which cause nuclear localization of the enzyme in yeast cells [1,6–9]. In addition, the N-terminus of Apn1 contains a mitochondrial localization signal, with localization requiring binding of Apn1's C-terminus to Pir1 protein [1,3]. Apn1 is an important player in base excision repair (BER) both in the nucleus and the mitochondrion [10]. It is also a major AP endonuclease in *S. cerevisiae* (responsible for approximately 97% of cellular AP endonuclease activity). In contrast, Endo IV is responsible for only about 5–10% of the *E. coli* cellular AP endonuclease activity [1–4,6,11–15].

Apn1 is a multifunctional enzyme with activities including AP endonuclease, 3′-phosphodiesterase, 3′-tyrosyl-DNA-phosphodiesterase, 3′-5′ exonuclease and endonuclease activity towards modified bases [1–5,15–17]. One active site is responsible for all enzymatic activities, and this site presumably contains three Zn^{2+} ions, which stabilize the tertiary structure of the protein and participate in catalysis [3,8,14]. However, there are data reporting tri-nuclear divalent metal active site of wild-type Endo IV containing two Zn^{2+} ions and one

Abbreviations: AP, Apurinic/apyrimidinic; BER, Base excision repair; F, (3-Hydroxytetrahydrofuran-2-yl)methyl phosphate; 2-aPu, 2-Aminopurine; MD, Molecular dynamics; ODN, Oligodeoxyribonucleotide

* Corresponding author at: Institute of Chemical Biology and Fundamental Medicine, Siberian Branch of the Russian Academy of Sciences, Lavrentyev Ave., 8, Novosibirsk, 630090, Russian Federation. Tel.: +7 383 363 51 75.
E-mail address: fedorova@niboch.nsc.ru (O.S. Fedorova).

http://dx.doi.org/10.1016/j.bbagen.2015.03.001
0304-4165/

Fig. 1. Alignment of the conserved regions of the amino acid sequences of *S. cerevisiae* Apn1 (P22936), *E. coli* Endo IV (P0A6C1), *Bacillus anthracis* Endo IV (Q81LV1), and *Thermotoga maritima* Endo IV (Q9WYJ7). Magenta and violet—α-helixes and β-sheets, respectively. Blue—amino acid residues involved in Zn^{2+} ions coordination. Asterisks denote identical amino acids. Dots and colons denote two and three conserved amino acids among the presented protein sequences from four organisms, respectively.

Mn^{2+} ion [18]. Apn1 and Endo IV were shown to substitute each other in cell cultures, suggesting these enzymes are able to repair the same spectrum of damages and carry out similar functions [1,5,6,9,19].

Despite the absence of crystal data for Apn1, the functions of some conserved amino acids proved to be distinct in Endo IV and Apn1 [5,20]. For instance, Glu-145 in Endo IV is involved in DNA binding and coordination of the Zn-cluster; whereas, the conserved Glu-158 of Apn1 is believed to only coordinate Zn^{2+} ions [1,5]. Amino acid substitutions of E145G in *E. coli* Endo IV and E158G in *S. cerevisiae* Apn1 were reported to completely eliminate DNA repair functions [1]. In the *Caenorhabditis elegans* APN-1 homolog the conserved Glu-261 residue corresponds to Glu-145 of *E. coli* Endo IV, which is involved in coordinating Zn^{2+} ions in the active site pocket. When this residue (Glu-261) is substituted with Gly, *C. elegans* APN-1 fails to rescue the DNA repair defects of mutant cells *S. cerevisiae apn1*Δ *apn2*Δ *tpp1*Δ as shown by cross-species complementation analysis [21]. Purification of E261G APN-1 from *C. elegans* yielded a truncated polypeptide and Glu-261 is believed to take part in maintaining the protein structure [21]. Also varying amino acid functions are found for Asp-179 and Val-143 in Endo IV, and Asp-192 and Val-156 in Apn1, respectively [5,20]. Interestingly, substituting Val-156 with Glu in Apn1 leads to a three-fold reduction in protein half-life as compared to WT Apn1, and retention of enzymatic activity up to 72 °C. A similar substitution of Val-143 with Glu in Endo IV results in defective repair capacity, independent of its steady-state expression levels [20]. As reported in Ref. [22], His-69 residue is involved in Zn1 ion coordination in the active site of *E. coli* Endo IV. Since conserved His-69 in *E. coli* Endo IV corresponds to His-83 in *S. cerevisiae* Apn1 (see Fig. 1), we hypothesized that the latter amino acid residue participates in metal ion coordination within the active site of yeast Apn1, thereby affecting DNA substrate binding and its enzymatic conversion. In the study, we focused on abasic site cleavage by mutant AP endonuclease H83A Apn1 during BER pathway.

2. Materials and methods

2.1. S. cerevisiae WT and H83A Apn1 isolation

WT and H83A Apn1 expression and purification were carried out as previously described except for the purification step on the HiTrap-Ni^{2+}-chelating column (GE Healthcare), which was not required for H83A mutant (for details see Supplementary Data, Fig. S1) [15,23].

2.2. Oligonucleotide substrates

Oligodeoxyribonucleotides (ODNs) were synthesized and purified as previously described [23]. The fluorescent 2-aPu probe was located either on the 5′- (upstream) or 3′-side (downstream) of an abasic site. ODN duplexes are presented in Table 1 (for details see Supplementary Data).

2.3. Stopped-flow measurements

Fluorescence measurements were carried out using microvolume stopped-flow spectrometers (models SX.18MV and SX.20, Applied Photophysics, UK) as described in Ref. [24]. Detection of intrinsic Trp fluorescence (Schott filter WG320, Germany) was at $\lambda_{em} > 320$ nm, with λ_{ex} being 280 nm [23]. Detection of 2-aPu fluorescence was taken at $\lambda_{ex} = 310$ nm and $\lambda_{em} > 370$ nm (filter LG-370-F, Corion,

Table 1
Sequences of oligonucleotide duplexes used as substrates and products of Apn1.

Shorthand	Sequence*
AP *or* ***F***	5′C-T-C-T-C-↓**X**-C-C-T-T-C-C3′ 3′G-A-G-A-G-C-G-G-A-A-G-G5′
AP(2-aPu) *or* ***F(2-aPu)***	5′C-T-C-T-C-↓**X**-**Y**-C-T-T-C-C3′ 3′G-A-G-A-G-C-C-G-A-A-G-G5′
(2-aPu)AP *or* ***(2-aPu)F***	5′C-T-C-T-**Y**-↓**X**-C-C-T-T-C-C3′ 3′G-A-G-A-C-C-G-G-A-A-G-G5′
P1	5′C-T-C-T-C-OH3′ 5′p**F**-C-C-T-T-C-C3′ 3′G-A-G-A-G -C -G-G-A-A-G-G5′
P2	5′C-T-C-T-**Y**-OH3′ 5′p**F**-C-C-T-T-C-C3′ 3′G-A-G-A - C - C - G-G-A-A-G-G5′
P3	5′C-T-C-T-C-OH3′ 5′p**F**-**Y**-C-T-T-C-C3′ 3′G-A-G-A-G - C - C - G-A-A-G-G5′
(2-aPu)G	5′C-T-C-T-**Y**-**G**-C-C-T-T-C-C3′ 3′G-A-G-A-C-C-G-G-A-A-G-G5′

* Modified nucleotides are **X** and **Y**, where **X**—regular abasic site (AP) or its tetrahydrofuran derivative (F); **Y**—2-aminopurine (2-aPu). Arrows indicate the site of Apn1 cleavage.

USA) [25]. All measurements were conducted at 25 °C in reaction buffer (BER buffer) containing 100 mM HEPES–KOH (pH 7.6) and 100 mM KCl. When fluorescence intensity of 2-aPu being registered, a substrate concentration was 1.5 μM and the protein concentration was varied from 0.5 up to 3.0 μM. Each kinetic trace is an averaging of five independent experiments. Cell volume is 20 μl and optical path is 2 mm. Dead time of the stopped-flow instruments were 1.38 (SX.18MV) and 1.1 (SX20) ms.

2.4. Kinetic data analysis

Global nonlinear least-squares fitting was performed using DynaFit software (BioKinLtd., USA) [26]. The fitting procedure was based on the consequential spreading of time slot and complication of the kinetic mechanism [24,27,28]. Minimal kinetic scheme describing experimental data was fitted and values of rate constants for individual step of the process were calculated (for details see Supplementary Data).

2.5. Steady-state fluorometry

Steady-state fluorescence measurements were conducted using a Cary Eclipse fluorescence spectrophotometer (Varian Incorporated, Australia) in thermostatic cell with optical path of 1 cm at 25 °C.

2.5.1. 2-aPu fluorescence measurements

The 2-aPu fluorescence kinetic traces upon H83A Apn1 interaction with ***(2-aPu)AP*** substrate (1.5 μM) were registered at $\lambda_{ex}^{2-\,aPu} =$ 310 nm and $\lambda_{em}^{2-\,aPu} =$ 368 nm at the different concentrations of the enzyme from 0.5 up to 3.0 μM with 0.25 μM step. Excitation and emission slit widths were 5 nm. Operating voltage was 800 V. Time between the mixing of reagents and the start of fluorescence registration was about 30 s in all cases.

2.5.2. Fluorescence titration of H83A Apn1 with synthetic ODNs mimicking endonuclease reaction products

Fluorescence equilibrium titration of H83A Apn1 was carried out at $\lambda_{ex} = 280$ nm and $\lambda_{em} = 350$ nm as described in Ref. [23]. Mixture of three ODNs mimicking AP endonuclease reaction product was prepared; sequences of products are presented in Table 1. Solution of H83A Apn1 (1.5 μM) in BER buffer was titrated with product solution like it was carried out with WT Apn1 [23]. Equilibrium association constants of H83A Apn1 bindings with ***P1***, ***P2***, and ***P3*** were estimated as described in ref. [29] (for details see Supplementary Data).

2.6. AP endonuclease assay

The *in vitro* DNA cleavage time course experiments were performed as previously described [23] (for details see Supplementary Data). Importantly, to quench the process, reaction mixture aliquots (2 μl) were added to the loading dye solution containing 7 M urea at defined time points. It should be noted that the same way of termination of the reaction is not suitable in the case of WT Apn1 catalysis due to its high enzymatic activity [23].

2.7. Determination of Zn (II) content

Zn (II) content was determined using Zn (II) chelating fluorophore, FluoZin-3 (registered trademark of Molecular Probes Inc., Life Technologies, USA), which is highly specific to Zn (II) ions ($\boldsymbol{K_d} \approx 15$ nM) [30,31]. Initially, fluorescence emission spectra of FluoZin-3 (10 μM) solution mixed with 0.1% SDS were recorded at every $ZnCl_2$ concentration increase step, from 0 to 1500 nM. Next, fluorescence emission spectra of solutions containing H83A Apn1 (100–400 nM, with 100 nM step) incubated in a mixture containing 0.1% SDS (20 min at 85 °C) were recorded. Fluorescence emission was observed at wavelengths from 500 to 650 nm; the excitation wavelength of FluoZin-3/Zn^{2+} complex, $\lambda_{ex}^{FluoZin-3/Zn^{2+}}$, was 490 nm. Following this, the fluorescence intensity versus concentration was plotted. The slope ratio between calibration and H83A Apn1 was in stoichiometry of Zn^{2+} ions per protein molecule. Experiments were conducted utilizing a Cary Eclipse fluorescence spectrophotometer (Varian Incorporated, Australia) in temperature controlled cell with an optical path of 1 cm at 25 °C, operating voltage was 890 V, slit width 2.5 nm. Results of three independent experiments were averaged.

2.8. Homology modeling

The amino acid residue sequences of Apn1 and Endo IV orthologs from bacterial, fungal, and metazoan organisms were downloaded from the UniProt database [32]. A sequence alignment was then performed with the protein homology/analogy recognition engine (Phyre) [33]. Multiple protein sequence alignments were carried out using Clustal Omega software [34]. The structure of Endo IV (PDB: 1QTW [22]) was used as the main template to build a homology model of the central region of Apn1 using the ensemble fold recognition method. During homology modeling we built a 3D structure of Apn1 for amino acid sequence from 16 to 293 residues, since the N-terminus and C-terminus of Endo IV are shorter than those of Apn1.

2.9. Molecular dynamics simulations

The H83A mutation was inserted using the Structure Editing tool of UCSF Chimera [35]. Positions and the number of catalytic Zn^{2+} ions were calculated using RaptorX-Binding server [36] and metal positions were verified by CheckMyMetal server [37]. When editing the initial PDB file employed for modeling, Zn^{2+} ions were placed in the Apn1 structure according to the general principles underlying metal ion coordination in proteins [18,38,39], and are based on Refs. [18,40]. The resulting structure was subjected to minimization, while metal ions and amino acids were allowed to adopt an optimal conformation.

DNA duplex structure was derived by editing precursor one, reported in Ref. [18] (PDB ID: 2NQJ), using UCSF Chimera [35]. The final required 12-mer duplex containing the 5′-mismatched 2-aPu residue close to the F site, which is flipped-out of the DNA helix, was derived from an initial 15-mer duplex.

The final refinement was performed by 500 ps of simulated annealing using the AMBER 12 molecular modeling suite [41]. The mutant structure was finally validated using the PDB validation module of AmberTools 13 [42]. The AMBER force field parameters

for the 2-aminopurine-5′-phosphate residue were taken from Ref. [43], Zn^{2+} parameterization was done according to [44]. A 10 ns molecular dynamics simulation was performed utilizing the AMBER 12 molecular dynamics modeling software with GPU accelerated code [45,46] using the ff99SB force field [47,48] and the analytical implicit solvent model, with an integration time step of 1 fs. The system was gradually heated from 1.2 K to 300 K over 2500 ps and equilibrated at room temperature. A classic molecular dynamics trajectory was generated in the NTV ensemble with harmonic restraints of 0.001 kcal/Å^2 for the protein atoms, 0.25 kcal/Å^2 for atoms of the terminal nucleotides, and 0.0025 kcal/Å^2 for the rest of the DNA atoms. Coordinates of each atom of the system (snapshots) were saved every 1 ps. Molecular graphics, MD movie generation and analyses were performed with the UCSF Chimera package [35]. The structures were visualized using the PyMOL (Schrödinger, LLC, New York) [49] molecular graphics system.

3. Results and discussion

3.1. 2-aPu fluorescence of DNA substrates reveals delays of the catalytic step after the substitution of His-83 with Ala in Apn1

In this study we focused on the role of His-83 in Apn1 catalysis. The conformational rearrangements in Apn1 could not be followed due to small changes of intrinsic Trp fluorescence. Detection of 2-aPu fluorescence in DNA substrates was used to study the conformational dynamics of damaged DNA during the interaction with H83A Apn1. The fluorescent analog of a heterocyclic base, 2-aPu, was incorporated into the DNA strand in close proximity to the damaged site, as in previous studies [23,25,50–54].

Pre-steady state kinetic traces of 2-aPu fluorescence intensity were recorded during H83A Apn1's interaction with ***AP(2-aPu)*** and ***F(2-aPu)*** substrates, using stopped-flow technique under single-turnover conditions for different enzyme concentrations (Fig. 2). With regard to the lesions used, regular AP sites tend to undergo spontaneous β-elimination due to equilibrium formation of an acyclic isomer. To avoid spontaneous substrate degradation, the synthetic analog of abasic site, F, was utilized, as in previous studies [27,29,50,55–59].

In Fig. 2 2-aPu fluorescence intensity decreased up to 1 s in both cases. Such fluorescence behavior, resulting from local hydrophobicity increase, is evidence for enzyme–substrate complex formation, when DNA is surrounded by more hydrophobic amino acid residues of the enzyme rather than the polar aqueous solution in the case of free DNA. The subsequent increase of 2-aPu fluorescence intensity, presumably, corresponds to catalytic stage completion, when the enzyme–substrate complex is converted into an enzyme-product complex. Comparing kinetic traces for 1:1 ratio of the enzyme to the substrate, we found that this process took place in the time range up to 200 s for ***AP(2-aPu)*** and 40 s for ***F(2-aPu)***. The next stage, characterized by a significant decrease in curve slopes, appears to be the dissociation of the enzyme-product complexes. H83A Apn1 appears to cleave substrates ***AP(2-aPu)*** and ***F(2-aPu)*** in several stages. These processes may be described, in principle, using one kinetic mechanism (see Scheme 1) derived by global non-linear fitting of the experimental data. This kinetic scheme contains one irreversible step and three or four reversible ones for ***F(2-aPu)*** and ***AP(2-aPu)*** substrates, respectively. The first two equilibriums (phases I and II, Fig. 2A–B), more likely, represent the initial nonspecific binding and subsequent specific recognition of the F or AP sites. The irreversible step (phase III), characterized using the rate constant k_3, is the catalytic chemical reaction of 5′-phosphodiester bond incision within the AP site, i.e. $k_3 = k_{cat}$. In the case of ***AP(2-aPu)***, phase IV appears to be a conversion of the enzyme–product complex to different one, which dissociates with product release at the next stage. The final equilibrium (phase V) is the dissociation of the enzyme-product complex.

Fig. 3 represents the kinetic traces obtained during the interactions of WT enzyme and H83A Apn1 with ***X(2-aPu)*** (***X*** = AP or F) substrates. It is seen that WT Apn1 cleaves DNA substrates independently on damage, whereas H83A Apn1 incises synthetic F-containing substrates rather than regular AP-containing ones. The values of kinetic constants obtained in the fitting procedure are presented in Table 2. This and other data obtained earlier [23] show that WT Apn1 cleaves these substrates faster. For instance, k_3 for interaction of WT with ***F(2-aPu)*** substrate is 0.33 s^{-1}; whereas k_3 for H83A in the same case is 0.073 s^{-1} (see Table 2). Comparing interactions of WT and H83A Apn1 with ***AP(2-aPu)*** substrate, k_3 is 0.53 s^{-1} and 0.043 s^{-1}, respectively. These data reveal a 5- and 12-fold reduction in H83A mutant catalytic activity, on ***F(2-aPu)*** and ***AP(2-aPu)*** substrates, respectively, when compared with WT Apn1. This indicates an important role of His-83 in catalysis. These findings highlight the H83A Apn1 mutant's defective catalysis, which is a result of substituting the bulky, positively charged His-83 residue with the small nonpolar Ala residue. The His-83 residue is involved in Zn^{2+} ion coordination, and the smaller Ala residue cannot substitute this function.

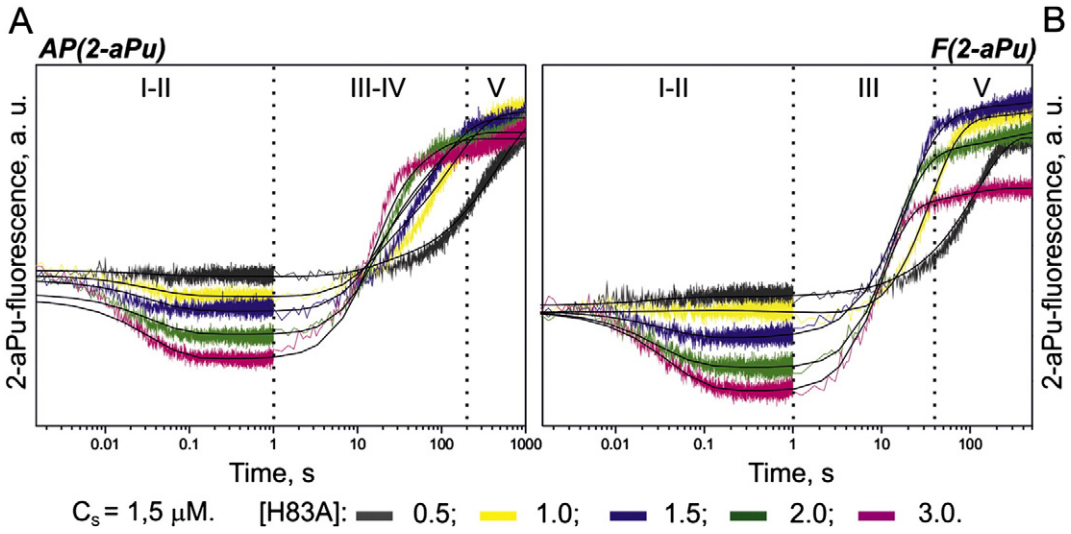

Fig. 2. Conformational dynamics of (A) ***AP(2-aPu)*** and (B) ***F(2-aPu)*** substrates during the interaction with H83A Apn1. Areas enclosed between dotted lines designate elementary stages of the process, which are numbered according to stages in the kinetic Scheme 1.

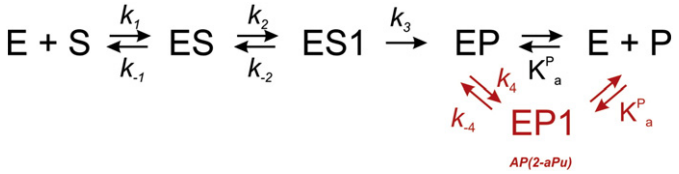

Scheme 1. Minimal kinetic mechanism of abasic site cleavage by H83A Apn1.

K_a^P values are estimated with low accuracy due to curve misphasing, in stopped-flow experiments, during long reaction times. Therefore, to accurately measure the affinity of H83A Apn1 to products, K_a^P values were determined using steady-state fluorescence titration of the protein with mixture of ODNs mimicking the reaction products (see Supplementary Fig. S2). As seen in Table 2, WT Apn1 and H83A Apn1 have identical tendencies to associate with ODNs mimicking reaction products. The His-83 to Ala substitution does not affect this association for both F-containing DNAs: ***(2-aPu)F*** and ***F(2-aPu)***. On the other hand, for the AP-containing DNAs, no influence is seen for ***(2-aPu)AP***, but a high influence is observed for ***AP(2-aPu)***. Such a difference has occurred due to smaller k_{-1} value compared to cases of other DNA substrates. According to our previous data [50], ***AP(2-aPu)*** substrate has a better structure for catalysis with human AP endonuclease APE1. Thus, His-83 may be responsible for Apn1's specificity to DNA. The His-83 residue, most likely, is not involved in subsequent DNA structure changes following substrate cleavage and enzyme-product complex (EP) formation (see step 3 in **Scheme** 1).

3.2. AP endonuclease assay directly reveals the differences in H83A Apn1 catalysis depending on DNA structure

The AP endonuclease assay was carried out using denaturing PAGE with the reaction mixture containing ^{32}P-labeled AP- or F-containing strand in DNA duplexes and H83A Apn1, in BER buffer (see Supplementary Fig. S3). Concentrations of ODNs and H83A Apn1 were 1.5 μM. Analysis of results obtained supported stopped-flow data and showed that H83A Apn1 preferentially cleaves DNA substrates containing the F site, rather than AP-containing ones (Fig. 4A). The value V_0^F/V_0^{AP}, estimated as the ratio of slopes to initial regions of corresponding traces, was 2.4. It means that cleavage at the ***F*** site proceeds 2.4 times faster than at the ***AP*** site (Fig. 4B). The ratio $V_0^{F(2\text{-}aPu)}/V_0^{AP(2\text{-}aPu)}$ was 3.7.

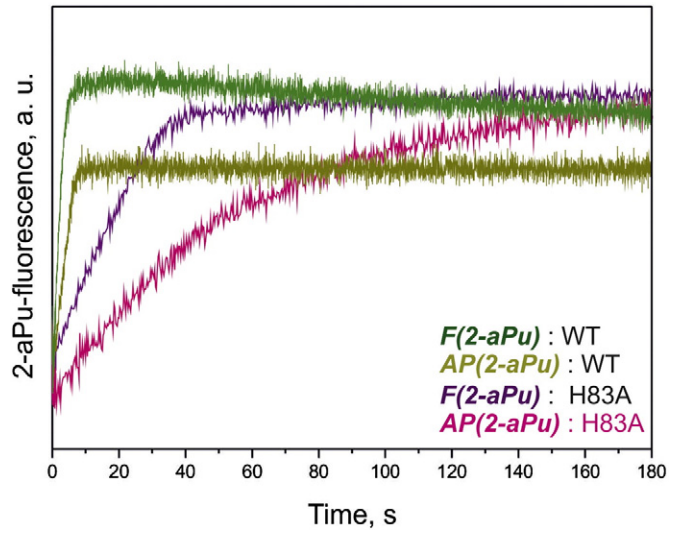

Fig. 3. 2-aPu fluorescence kinetic traces upon interaction of WT enzyme and H83A Apn1 with ***AP(2-aPu)*** and ***F(2-aPu)*** substrates. [Enzyme] = [DNA] = 1.5 μM.

The main difference of the abasic site used is absence or presence of OH-group at C1′ atom. In the case of regular AP site, there is OH-group at C1′ atom, therefore, "close" and "open" forms of the deoxyribose ring are formed, with equilibrium shifted to "close" conformation. Synthetic abasic site, F, does not have this OH-group, therefore, F can exist in "close" conformation only. Probably, this fact can explain the catalytic differences observed. Interestingly, WT Apn1 was found to cleave DNA substrates independently of both the nature of the lesion (regular AP site or its synthetic analog F) and mismatch location relative to the damaged site (upstream or downstream 2-aPu residue) (see ref. [23] and Fig. 4A). Moreover, WT Apn1 operated according to a scheme identical to that of H83A Apn1 interaction with the ***F(2-aPu)*** substrate [23]. These findings highlight the catalytic significance of His-83 residue in *S. cerevisiae* Apn1. The distinction between WT and H83A Apn1 suggests that the His residue mutation in position 83 dramatically influences the structure of the enzyme's active site.

Interestingly, ***(2-aPu)X*** duplexes were not cleaved by H83A Apn1 (see Supplementary Data, Figs. S3–S4). This indicates the structure of mutated enzyme is changed significantly, when His-83 substituted with Ala, and the enzyme is not able to adjust to the highly bent ***(2-aPu)X*** DNA.

3.3. His-83 residue plays a crucial role in Apn1 catalysis

It was previously shown that modification of bases located at the 5′-side of the AP site had a negative influence on human APE1 activity [50, 58]. Since, the AP endonuclease assay using PAGE found no activity of H83A Apn1 on ***(2-aPu)X*** duplexes (see Supplementary, Fig. S4), it was interesting to study conformational dynamics of the duplexes to clarify whereby DNA incision does not occur. In addition, do either the structural features of DNA or His substitution with Ala lead to weak divalent metal ion coordination? What stage of the process is locked: DNA binding or DNA incision?

The kinetic traces of 2-aPu fluorescence upon H83A Apn1 interactions with ***(2-aPu)X*** are presented in Fig. 5 [A—data obtained by stopped-flow technique for ***(2-aPu)F***, B—steady-state fluorescence data obtained for ***(2-aPu)AP***]. For ***(2-aPu)AP*** interaction stopped-flow measurements, 2-aPu fluorescence intensity was recorded using steady-state fluorometry to avoid stray effects as a result of the

Table 2
Rate and equilibrium constants for WT* and H83A Apn1 interactions with DNA substrates ***F(2-aPu)*** and ***AP(2-aPu)***.

Apn1	***H83A***		***WT****	
Constants	DNA shorthand			
	F(2-aPu)	***AP(2-aPu)***	***F(2-aPu)***	***AP(2-aPu)***
k_1 (M^{-1} s^{-1})	$(2.40 \pm 0.04) \times 10^5$	$(4.9 \pm 0.1) \times 10^5$	$(1.7 \pm 0.2) \times 10^5$	$(4.5 \pm 0.1) \times 10^5$
k_{-1} (s^{-1})	24.9 ± 0.2	26.0 ± 0.08	3.8 ± 0.6	0.35 ± 0.08
K_1**	9.6×10^4	1.9×10^4	4.5×10^4	12.9×10^5
k_2 (s^{-1})	2.5 ± 0.1	1.6 ± 0.04	1.3 ± 0.1	10 ± 1
k_{-2} (s^{-1})	0.049 ± 0.002	0.085 ± 0.001	0.10 ± 0.02	2.2 ± 0.1
K_2**	51	18.8	13	4.6
k_3 (s^{-1})	0.073 ± 0.002	0.043 ± 0.001	0.33 ± 0.01	0.53 ± 0.01
k_4 (s^{-1})		0.096 ± 0.002		
k_{-4} (s^{-1})		0.055 ± 0.01		
K_a^S, M^{-1}***	5.0×10^5	3.7×10^5	6.3×10^5	7.2×10^6
K_a^P, M^{-1}****	6.7×10^4	N/A	3.3×10^4	N/A

* Data are taken from Ref. [23].
** $K_i = k_i / k_{-i}$.
*** K_a^S is the equilibrium association constant calculated from stopped-flow data according to equation $K_a^S = K_1 \times (1 + K_2)$ for two-step binding mechanism (see Scheme 1).
**** K_a^P is the association constant calculated from fluorescence titration data (experimental error does not exceed 30%).

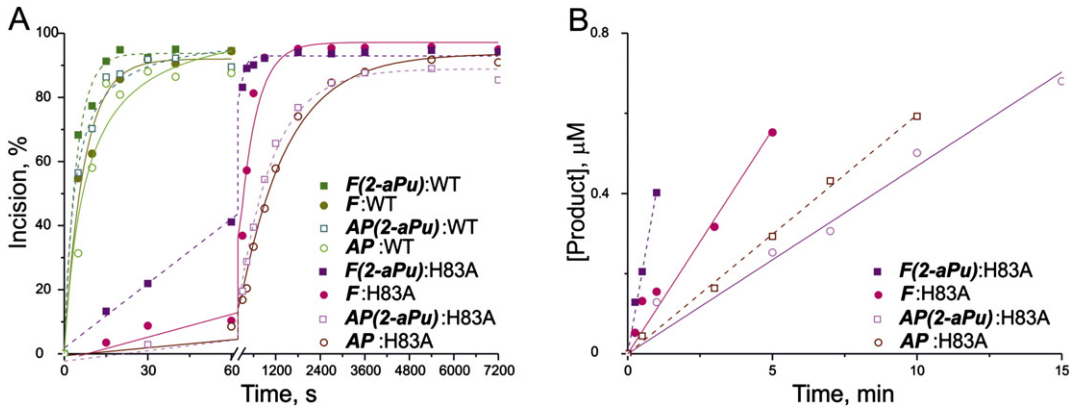

Fig. 4. AP endonuclease assay of WT [23] and H83A Apn1 on DNA substrates by denaturing PAGE. (A) Incision of F-containing substrates is signed as solid circles and squares; that of AP-containing ones are signed as open figures. Data for ***AP*** and ***F*** substrates are presented as solid line, and for ***AP(2-aPu)*** and ***F(2-aPu)*** as dashed line. Olive, green, dark cyan and dark yellow represent WT data, and wine, purple, light magenta and pink—H83A data. (B) Linear fitting of initial regions of the traces, which slopes were taken for V_0. [Enzyme] = [DNA] = 1.5 μM.

biomolecules exposed to long and continuous radiation. Fluorescence intensity gains were observed up to 1000 s (1.5 μM enzyme), when recording intensity changes for ***(2-aPu)X*** substrate. The long lasting fluorescence growth may represent only DNA binding to the enzyme, and the transition of the initial enzyme–substrate complex into a non-catalytically active state, as revealed by PAGE analysis of AP endonuclease assay with ***(2-aPu)X*** DNA (see Supplementary, Figs. S3–S4).

Behavior of 2-aPu fluorescence intensity in both processes is similar, with superposition of the kinetic traces showing their absolute conformity. This indicates the same enzyme actions on the DNA substrates (Fig. 6).

Altogether, our results indicate a tendency of H83A Apn1 to incise DNA duplexes in the following order: ***F(2-aPu)*** ≈ ***F*** ***AP(2-aPu)*** ≈ ***AP*** ***(2-aPu)F*** ≈ ***(2-aPu)AP***. Earlier studies on the cleavage of damaged DNA by human BER enzymes, including 8-oxoG DNA glycosylase 1 (hOGG1) and AP endonuclease 1 (APE1), reported that mismatches upstream of the lesion reduced enzymatic activities to a greater extent than downstream ones [50,55,58,60]. The DNA backbone containing an upstream mismatch to AP site was highly bent and distorted in active site of APE1, resulting in a decrease in catalysis rate [50,58]. It should be noted that an upstream mismatch decreases both the affinity of WT APE1 to the damaged DNA and the incision rate of the abasic site F, as compared to a natural authentic AP site [29,50]. Our studies on yeast WT Apn1 showed that upstream or downstream mismatches relative to the abasic site had no influence on the incision of damaged DNA [23]. In view of these data, it was interesting to examine the effect of mismatch upstream of the damaged site and, at the same time, follow the conformational dynamics of ***(2-aPu)F*** substrate during the interaction with H83A Apn1.

The data obtained for interactions of H83A Apn1 with both ***X(2-aPu)*** and ***(2-aPu)X***, which practically appear not to lead to the formation of incised products, were fitted to a minimal kinetic scheme (Scheme 2). The values of kinetic constants, which were fitted according to this scheme, are presented in Table 3. Interestingly, the affinity of H83A Apn1 to both ***X(2-aPu)*** and ***(2-aPu)X*** substrates is almost equal (see Tables 2–3). It is worthwhile to note that the catalytic stage of H83A Apn1 interacting with ***X(2-aPu)*** substrate results in an irreversible incision of damaged DNA. On the other hand, during its interaction with ***(2-aPu)X*** the observed catalytic stage is the irreversible release of DNA. In this case, the released DNA, although still damaged, is

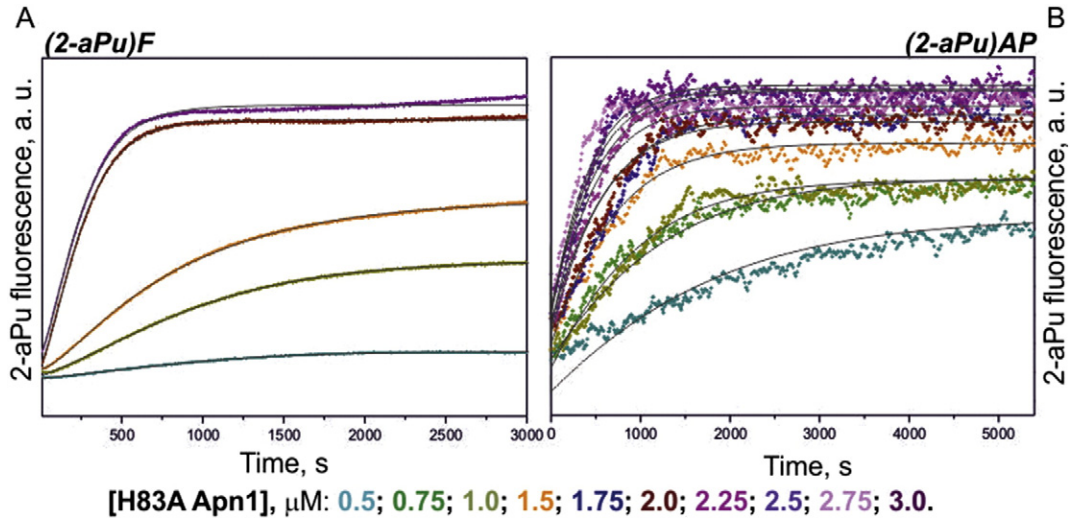

Fig. 5. Kinetic traces of H83A Apn1 interaction with (A) ***(2-aPu)F*** (stopped-flow technique) and (B) ***(2-aPu)AP*** (steady-state fluorometry) duplexes. In the case of ***(2-aPu)AP*** substrate, concentrations of H83A Apn1 were varied from 0.5 up to 3.0 μM with 0.25 μM step excluding 1.25 μM. In the case of ***(2-aPu)F*** substrate, concentrations of H83A Apn1 were 0.5, 1.0, 1.5, 2.0, and 3.0 μM. Concentration of DNA was constant and equal to 1.5 μM.

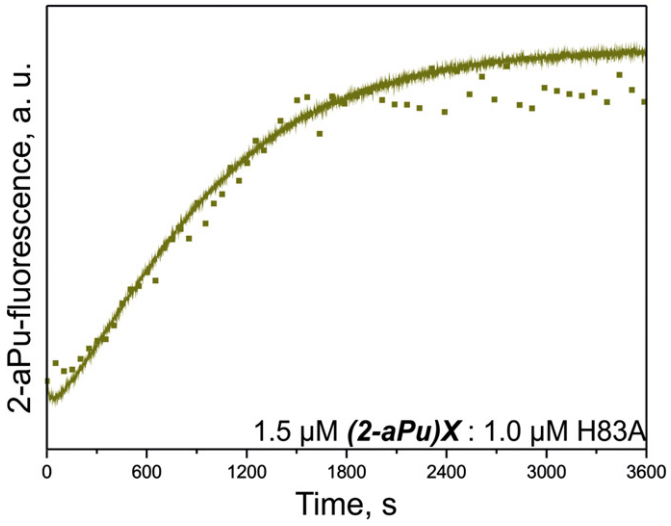

Fig. 6. Superposition of kinetic traces for 1.0 μM H83A interacting with 1.5 μM ***(2-aPu)X*** duplex (***X*** = ***AP*** or ***F***). Kinetic trace obtained for ***(2-aPu)F*** by stopped-flow technique is presented with solid line; that for ***(2-aPu)AP*** obtained by steady-state fluorometry is presented with squares.

modified from the previous DNA–H83A Apn1 complex (L1 in Scheme 2). However, the exact nature of this conversion will need to be established later.

To obtain additional information on H83A Apn1's affinity for non-cleavable duplexes, fluorescence titration of the enzyme with the ***(2-aPu)F*** duplex was performed using ***(2-aPu)G*** duplex as a control (see Table 1 and Supplementary Fig. S5). Association constant values were estimated as $K_a^{EL} = (1.5 \pm 0.5) \times 10^5\ M^{-1}$ for ***(2-aPu)F*** and $K_a^{EL} = (1.0 \pm 0.3) \times 10^5\ M^{-1}$ for ***(2-aPu)G***. For ***(2-aPu)F*** the value of K_a^{EL} was found to be in satisfactory agreement with K_a^{EL} obtained by stopped-flow pre-steady-state kinetics (Table 3).

H83A Apn1 had an affinity of $2.5 \times 10^5\ M^{-1}$ to the incision products of the ***(2-aPu)F*** duplex, which was determined by fluorescence titration. This proved to be higher than that of incised ***F(2-aPu)*** (see Table 2). Comparison of K_a^P values for WT enzyme and H83A Apn1 revealed identical affinities of both enzymes to ***(2-aPu)F*** products (***P2***) (see Supplementary Fig. S2).

3.4. Molecular dynamics of H83A Apn1

Molecular dynamics (MD) simulations of H83A Apn1 complexed with ***(2-aPu)F*** duplex were undertaken to identify Apn1 active site changes, which lead to significantly reduced catalytic activity. The MD simulations were aimed at answering whether either the His-83 substitution with Ala makes Apn1 inactive or the 5′-mismatch close to the abasic site causes such DNA distortions. These distortions are not compatible with the active site of the mutated enzyme preventing it from moving into the catalytic stage. The first part of the MD simulation work consisted of three logical steps: specifying amino acid coordination in an Apn1 molecule; constructing and optimizing the DNA structure bound to Apn1 (with F and 2-aPu residues located in the central part of the duplex); defining the position and quantifying Zn^{2+} ions at the enzyme's active site.

$$E + L \underset{k_{-1}}{\overset{k_1}{\rightleftharpoons}} EL \xrightarrow{k_2} E + L1$$

Scheme 2. Kinetic mechanism of H83A Apn1 processing of *(2-aPu)X* duplexes.

Table 3
Rate and equilibrium constants for H83A Apn1 interactions with 5′-mismatched DNA duplexes.

Shorthand	***(2-aPu)F***	***(2-aPu)AP***
k_1 ($M^{-1}\ s^{-1}$)	$(5.0 \pm 0.04) \times 10^6$	$(3.20 \pm 0.04) \times 10^6$
k_{-1} (s^{-1})	8.3 ± 0.1	11.4 ± 0.1
k_2 (s^{-1})	0.0059 ± 0.0001	0.0057 ± 0.0001
K_a^{EL}, M^{-1}*	6.0×10^5	2.8×10^5

* Equilibrium association constant (K_a^{EL}) was calculated from the equation $K_a^{EL} = k_1 / k_{-1}$ (see Scheme 2).

The results of initial WT Apn1 structure analysis validate and are consistent with data reported that *S. cerevisiae* Apn1 has the highest homology with *E.coli* Endo IV—42% (Fig. 1) (alignment results are presented in Supplementary Data—Alignment.pdf). Moreover, the enzymes share complete identity with respect to the nine conserved amino acid residues (His-69, His-109, Glu-145, Asp-179, His-182, His-216, Asp-229, His-231, Glu-261 in *E. coli* Endo IV and His-83, His-123, Glu-158, Asp-192, His-195, His-229, Asp-242, His-244, Glu-274 in *S. cerevisiae* Apn1, respectively) involved in metal binding, including His-83 in Apn1, which together are important for DNA incision activity (see Fig. 1, text highlighted in blue) [20,22].

Fig. 7 shows the overall view of WT Apn1 molecular complex with the ***(2-aPu)F*** DNA duplex. In addition, the localization of the amino acid residues within the enzyme's active site and Zn^{2+} ions is also shown.

Torsion angles of the modeled WT Apn1 structure were validated for allowable angles in protein structure. The H83A Apn1 structure resulting from homology modeling φ/ψ plot as defined by Ramachandran plot is shown in Supplementary Data (Fig. S6). The φ and ψ angles derived for polypeptide chain are in good agreement with classical distribution of allowed angles in protein molecules [61].

MD simulations of H83A Apn1 complexed with ***(2-aPu)F*** duplex and containing two or three Zn^{2+} ions in the active site were performed to determine whether His-83 substitution with Ala in Apn1 leads to a decrease in metal ion content. The DNA model contained a synthetic analog of the AP site and the upstream fluorophore residue, 2-aPu (Fig. 7A). 10 ns simulations at 300 K provided information on molecular system dynamics. MD movies for complexes, containing two or three Zn^{2+} ions in the active site of H83A Apn1 at 300 K, are presented in the Supplementary Data (Figs. S7–S8). The first model contained all three Zn^{2+} ions (denoted Zn1, Zn2, Zn3) similar to WT Apn1 [3,8]; the second one contained two metal ions: Zn2 and Zn3. MD movie analysis revealed that both models were stable and did not undergo complex destruction. MD simulations found that mobile protein domains were mainly exposed in solution. Hydrogen bonds within the terminal base pairs were occasionally broken. This is regular, stable behavior of molecular complexes during MD simulations. Both the tri- and bi-nuclear Zn^{2+}-cluster models evolved slowly from the initial run up stage to 4 ns, and were quite stable after 5 ns, as evidenced by two-dimensional root-mean-square deviation (r.m.s.d.) plots (Fig. S9A–B); overall, the r.m.s.d. of heavy atoms did not exceed 3.0 Å.

MD simulations showed that the synthetic abasic site, F, flipped-out from the DNA helix and located in WT Apn1's active site, had not undergone significant changes in its position (or conformation). Behavior of the 2-aPu residue located opposite dC on the 5′-side of the F residue was labile and was placed near a cavity formed by the F site flipping-out, with 2-aPu residue being able to change fluorescence intensity owing to variability in the environment.

Based on the data obtained, we hypothesized that metal ions in WT Apn1 molecule were coordinated as follows (Fig. 7B): Zn1 ion was coordinated with His-83, His-123, Glu-158 and oxygen atom of 5′-phosphate of the F site; Zn2 was coordinated with Asp-192, His-229, Glu-274, and another oxygen atom of the phosphate moiety; Zn3 was

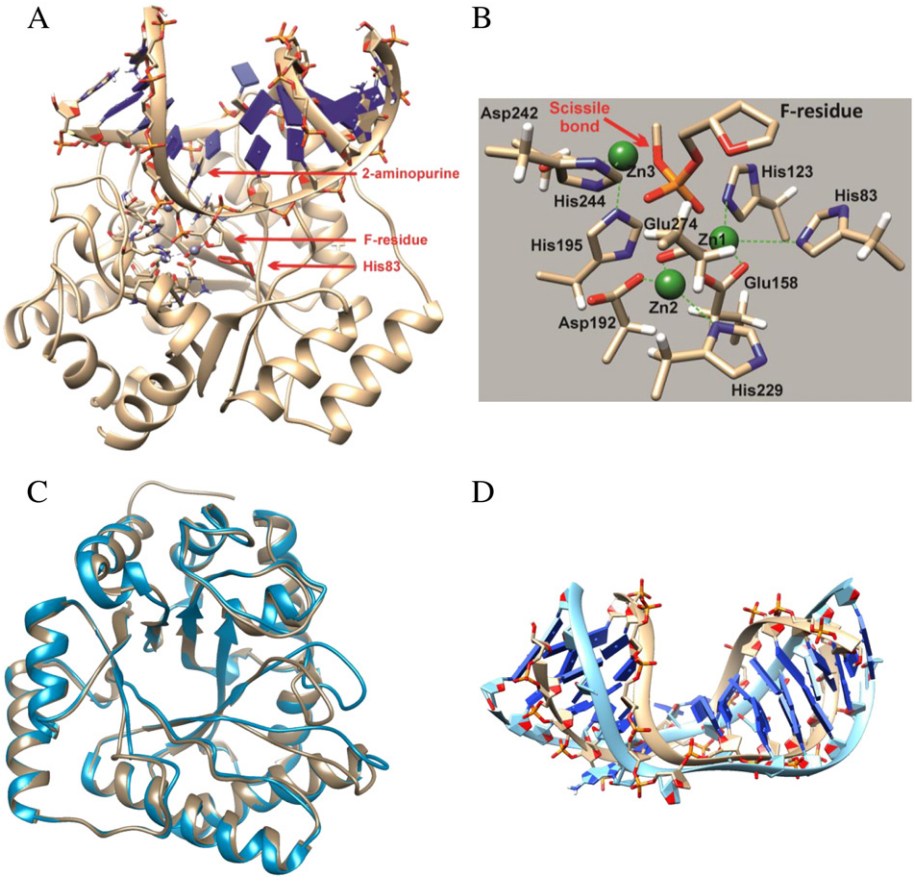

Fig. 7. Spatial structure of WT Apn1 complexed with F site in ***(2-aPu)F*** DNA duplex. The rest of the protein is shown as a schematic model. (A) An overall view of Apn1 molecular complex with DNA duplex, with Zn^{2+} ions shown in gray. (B) Active site residues localization. Zn^{2+} ions are shown as green CPK spheres, His-83, His-123, Glu-158, Asp-192, His-195, His-229, Asp-242, His-244 and Glu-274 amino acid residues forming the active site are shown in stick models colored according to the atom type (*khaki*, carbons; *blue*, nitrogens; *red*, oxygens; *brown*, phosphorus atoms). (C) A superposition of the endonuclease IV structure (PDB: 1QTW) that was used as template (*khaki ribbons*) as well as the final model for Apn1 (*sky blue ribbons*). The RMSD between 251 atom pairs for superpositioning of alpha carbon atoms in the protein is 0.493 Å. (D) A superposition for starting (*tan*) and final model for the DNA duplex (*sky blue*). Overall RMSD between all atoms in DNA is 3.682 Å.

complexed with His-195, Asp-242, and His-244. Tri-nuclear Zn-cluster formed an isosceles triangle, with distances between metal ions being Zn1–Zn2 (3.9 Å), Zn1–Zn3 (5.9 Å) and Zn2–Zn3 (6.0 Å). Such an arrangement of metal ions allowed them to perform multiple functions. On the one hand, Zn^{2+} ions coordinated phosphate moiety of the AP site, thereby stabilizing the flipped-out abasic sugar. As a result, a strong coordination bond was formed between the AP-DNA and the enzyme binding site. On the other hand, all three Zn^{2+} ions were involved in catalysis: Zn1 and Zn2 cooperated oxygen atoms of phosphate group, located near the bond to be cleaved, and attracted the electron density towards them, facilitating phosphodiester bond cleavage. When cleavage product formed, Zn3 ion seemed to interact with the 5′-side of the AP site-containing strand of the DNA product, stabilizing the leaving group.

As His-83 is involved in Zn1 coordination (see Fig. 7B), the substitution of this residue with Ala is expected to cause the metal ions to either change positions relative to that in WT Apn1, or be absent in the folded protein after its synthesis on the ribosome. Fig. 8 shows the superimposition of protein structures of both simulated systems. Both structures of the protein and DNA are slightly different from each other. Location of Zn2 ion changes insignificantly, while, Zn3 shows substantial shifts in position (12 Å).

MD simulations of the H83A Apn1 structure containing the two Zn^{2+} ions revealed an insignificant movement of Zn2 relative to DNA and amino acid residues involved in Zn2 coordination (Figs. 8–9A). Zn3 ion, on the other hand, is coordinated with Asp-242 and shifted 4.6 Å closer to the 5′-end of the F-containing DNA. In this position, Zn3 has a novel coordinating sphere consisting of Ala-161, Gly-162, Asn-240 and Asp-242 (Fig. 9B).

MD simulation of tri-nuclear Zn^{2+} H83A Apn1 structure found that the most substantial changes took place for the Zn3 ion. As seen in Fig. S8, immediately at the beginning of MD simulation, the Zn3 ion shifted along the DNA-binding groove of Apn1 towards the 5′-end of the F-containing DNA strand. Here, Zn3 left its coordination sphere and was released from H83A Apn1–DNA complex. Substitution of positively charged His-83 with nonpolar Ala led to Zn1 coordination weakening, followed by slight shifts in the metal ion relative to its original location. The result of Zn1 shifting means Glu-274 now has to coordinate both Zn1 and Zn2 ions instead of just the one Zn2 coordinated in WT Apn1 (Fig. 9C).

As seen in Fig. 7A, the flipped-out F site is tightly stabilized within the active site by an H-bond network formed by amino acid residues of the protein, with metal ions forming the “clip” between DNA and WT Apn1. Introducing a mutation at position 83 in Apn1 results in the disruption of active site geometry. Fig. 9 shows the localization of Zn^{2+} ions and amino acid residues of H83A Apn1 complexed with F-containing DNA duplex. The preferred coordination sphere of metal ions had a hexagonal geometry implying the presence of bound water molecules.

The structure obtained for H83A Apn1 complexed with the ***(2-aPu)F*** duplex revealed changes in the position and coordination of Zn1 ion as well as amino acid residues cooperating this metal ion, as compared

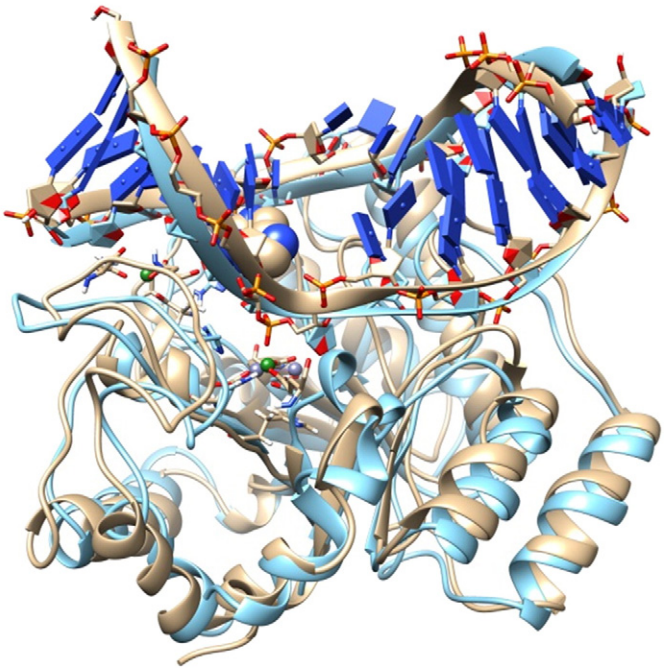

Fig. 8. Superimposition of MD snapshots for MD simulation of H83A Apn1–substrate DNA complex with three Zn^{2+} ions (*sky blue ribbons, Zn^{2+}—violet spheres*) and two Zn^{2+} ions (*khaki ribbons, Zn^{2+}—green spheres*).

with WT Apn1. These rearrangements induced weakening of oxygen atom coordination by the F site phosphate moiety, resulting in altered electron density distribution in the phosphate group. Therefore, catalytic activity of H83A Apn1 should decrease towards abasic DNA.

Our MD simulation data support and are in close agreement with data reported by J. Tainer and coauthors [18]. Apn1 from *S. cerevisiae* adopts an eight-stranded α–β barrel fold (TIM barrel), its binding to DNA is mediated by five R-loops and the active site contains three metal ions bound in a deep depression near the center of the barrel (Fig. 7) [18]. However, J. Tainer and coauthors reported Endo IV contains 2.05 zinc ions and 0.38 manganese ions per protein molecule [18]. Positions and coordination of divalent metal ions are substantial if not key aspects of Apn1 catalysis. In our study, computational modeling shows that all three Zn^{2+} ions, in the active site of WT Apn1, participate in coordination of the flipped-out abasic sugar. Moreover, the metal ions are also involved in transition state formation owing to the distribution of electron density within the phosphate group near the abasic site.

A key amino acid required for catalytic activity of Apn1 is the His-83 residue. The substitution of His-83 with Ala results in a significant decrease in the catalytic rate constant k_3, which characterizes the AP site incision rate. Such an effect seems to be caused by the distortion of AP site coordination in the transition state and, most importantly, the movement of Zn1 ion relative to 5′-phosphate moiety adjacent to the AP site. This movement causes disruption of the H-bond network followed by small fluctuations in Zn2's position and strong disturbances of Zn3 ion arrangement. It also plays a crucial part in DNA incision and stabilizes the leaving residue.

It is worthwhile paying special attention to the orientation of fluorescent probe, 2-aPu, within the DNA duplex. Data obtained reveals 2-aPu residue is sufficiently moveable within the complementary duplex opposite dC (Figs. S7–S8). Location of 2-aPu upstream of the AP site is suitable for recording DNA structural changes. This is similar to our case, where 2-aPu is located near a cavity formed as a result of the abasic sugar flipping-out of the DNA helix. Therefore, 2-aPu fluorescence intensity changes are expected to display rearrangements in DNA conformation, phosphodiester bond incision in the vicinity of the AP site, and product release from the DNA-enzyme complex. However, mismatch upstream of abasic site was earlier shown to affect incision activity of human APE1 [50,58]. When 2-aPu residue is opposite dC, similar to the ***(2-aPu)F*** duplex utilized, it results in a mismatched base pair (Figs. 8, S7–S8) [62]. It is worth pointing out that the 2-aPu residue is located in the region of an acutely bending DNA duplex, which is induced by enzyme binding. As a result the 2-aPu residue

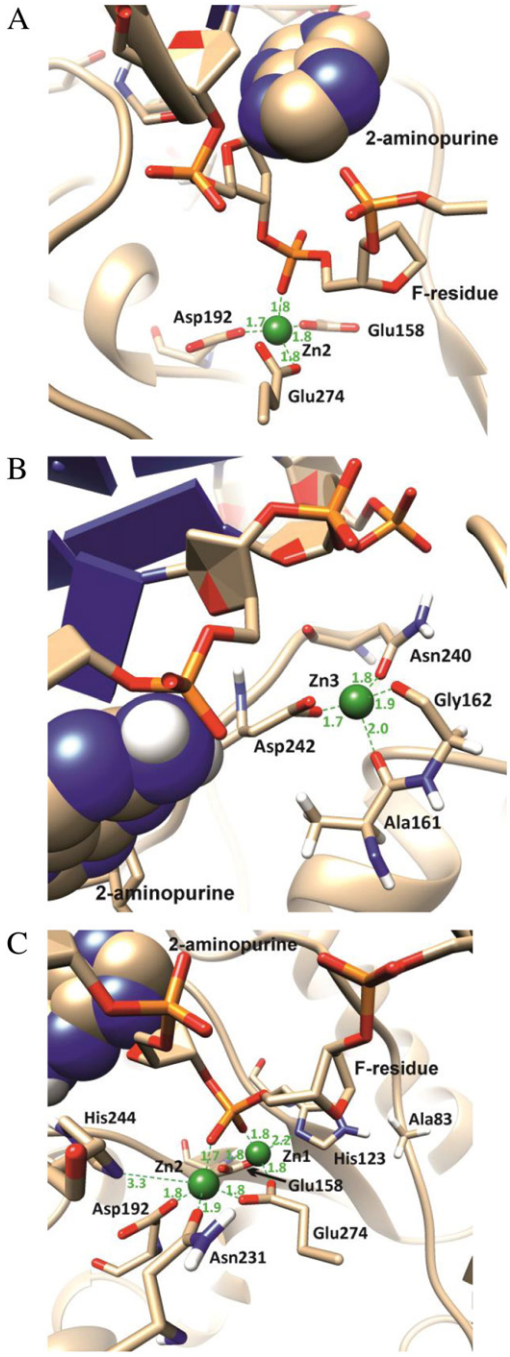

Fig. 9. Snapshots from the MD trajectory show the positions of the active site residues of H83A Apn1–substrate DNA complex. Geometry of metal coordination of Zn2 (A) and Zn3 (B) ions is displayed for MD simulation with two Zn^{2+} ions; geometry of Zn1 and Zn2 coordination (C) is displayed for MD simulation with three Zn^{2+} ions. Zinc ions are shown as green spheres, 2-aPu residue is shown in CPK spheres, F site, Glu-158, Asp-192, Glu-274 amino acid residues forming the active site are shown in stick models colored according to the atom type (*khaki*, carbons; *blue*, nitrogens; *red*, oxygens; *brown*, phosphorus atoms).

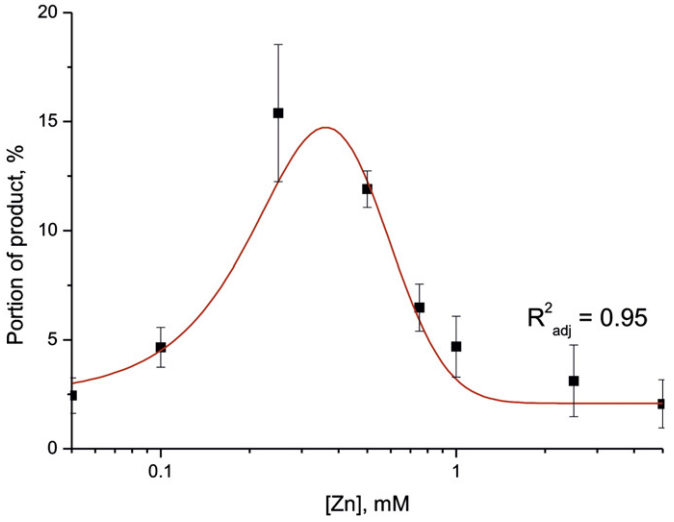

Fig. 10. The degree of ***(2-aPu)F*** duplex incision by H83A Apn1 depending on Zn^{2+} concentration.

moves towards the minor DNA groove and occupies the van der Waals volume intended for Zn3 ion. Therefore, Zn3 is displaced by 4.6 Å towards the 5′-end of the abasic DNA strand—a position, in which it cannot properly function. Thus, the mismatch located upstream of abasic site can influence the catalytic activity of H83A Apn1.

We conclude that a single amino acid substitution within the Apn1 active site leads to a cascade of changes in its geometry, causes removal and displacement of metal ions within the active site, and, finally, decreases the enzyme's catalytic activity. It should be noted that MD simulations of H83A Apn1 complexed with ***(2-aPu)F*** duplex also support the viewpoint of the presence of only two metal ions in the active site of the mutated enzyme. Mismatch location relative to the abasic site substantially influenced not only the DNA duplex geometry, but also the whole enzyme–substrate complex structure, and eliminated Apn1's incision activity.

3.5. Reconstruction of AP endonuclease activity of H83A Apn1 on non-cleavable DNA duplex

Inability of H83A Apn1 to incise abasic sites in various DNA substrates could be explained by the disruption of the Zn-cluster in the enzyme's active site. To test the hypothesis, we determined whether ***(2-aPu)F*** substrate cleavage by H83A Apn1 was dependent on Zn^{2+} concentration. As seen in Fig. 10, the Apn1 mutant incises ***(2-aPu)F*** substrate in the presence of 0.25–0.5 mM Zn^{2+} (about 80% of the product was formed within 5 min of the reaction start-time, see Supplementary, Fig. S4); whereas, 0.5 mM Mg^{2+} ions have an insignificant contribution in ***(2-aPu)F*** substrate incision (the incision rate was about 8% over 1.5 h) (see Supplementary Fig. S4).

In addition to determining the effect of Zn^{2+} concentration on AP endonuclease activity of H83A Apn1, the kinetic traces of H83A Apn1's interaction with ***(2-aPu)F*** substrate in the presence of 0.25 mM Zn^{2+} ions were also recorded (Fig. 11A). The presence of Zn^{2+} resulted in the restoration of H83A Apn1's AP endonuclease activity towards 5′-mismatched ***(2-aPu)F*** substrate. However, the mutant enzyme could not achieve the same level of activity for the ***(2-aPu)F*** duplex as it did for the 3′-mismatched ***F(2-aPu)*** substrate (Fig. 11B–D). Fig. 11B shows the conformational dynamics of the ***(2-aPu)F*** duplex interacting with H83A Apn1 in the presence and absence of Zn^{2+} ions, and with WT Apn1. Here one can see the regularity of catalytic stage acceleration in the following order: H83A Apn1 < H83A Apn1 + Zn^{2+} < WT Apn1 ≈ WT Apn1 + Zn^{2+}. The kinetic mechanism describing this interaction is exactly the same as ***F(2-aPu)*** interactions with WT Apn1 and H83A mutant (see Scheme 1). The values of kinetic constants corresponding to this mechanism are presented in Table 4. The catalytic rate of the recovered process is 2.7 times higher, compared with the same interaction in the absence of Zn^{2+} ions. The affinity of H83A Apn1 to ***(2-aPu)F*** in the presence of Zn^{2+} ions, is two times higher than without metal ions (see Tables 3–4). Moreover, the affinity of the recovered enzyme to ***(2-aPu)F*** is higher than that of H83A Apn1 to ***F(2-aPu)*** without Zn^{2+} ions. In other words, zinc ion deficiency within the active site of mutated Apn1 results in decreased affinity to damaged DNA substrates and depends on their spatial structures. Kinetic parameters of the interactions confirmed that the key difference lies in the catalytic stage (Tables 2–4). This fact sheds light on the participation of the His-83 residue in catalysis, where this residue is involved not only in Zn^{2+} coordination but also in the conversion of the substrate into the reaction product.

3.6. Assay of Zn^{2+} content in H83A Apn1 reveals two Zn^{2+} ions per molecule of mutant enzyme

All above findings confirm the hypothesis of weak Zn^{2+} coordination within the H83A Apn1 active site. To determine Zn^{2+} ion content in H83A mutant we used the Zn^{2+} chelator FluoZin-3, as described in Ref. [63] (see Supplementary Fig. S10). The fluorescence emission spectra of FluoZin-3/Zn complex were recorded either in the presence of H83A Apn1 or Zn^{2+} solutions of known concentrations. The comparison of fluorescence signals obtained for H83A Apn1 with the calibration curve, found 1.9 ± 0.2 Zn^{2+} ions per molecule of the mutant enzyme. This result supports our conclusion that the active site of the H83A mutant is depleted of Zn^{2+} ions compared to WT protein. Moreover, the analogous mutant H69A of *E. coli* Endo IV was shown to contain 1.7 zinc ions per protein molecule, while WT Endo IV contains 2.7 zinc ions, as measured by fluorescence emission of Zn/FluoZin-3 complex [63]. Endo IV was reported as the first TIM barrel structure containing a tri-nuclear Zn^{2+} cluster in its active site. Therefore, the suggestion that *S. cerevisiae* Apn1 contains an analogous Zn^{2+} cluster is very reasonable [3,8,14,64].

4. Conclusion

The location of 2-aPu, relative to the damage, was found to play a crucial role in DNA incision by H83A Apn1. Hence, when 2-aPu was located downstream of the damage, ***X(2-aPu)*** substrates were incised by H83A Apn1, but in contrast, the enzyme could not cleave ***(2-aPu)X*** duplexes. It should be noted that the structures of ***(2-aPu)X*** duplexes demonstrated a dramatic deviation from both canonical B-DNA, as well as ***AP*** or ***F*** substrate structures [50]. At the same time DNA helix in the ***AP(2-aPu)*** substrate is distorted to the smallest degree, and this substrate is found to be the most flexible DNA substrates tested [50]. In addition, similar results were reported earlier for human APE1, supporting the hypothesis that a mismatch upstream of the abasic site, has a dramatic effect on AP endonuclease incision activity on the damaged DNA [50,58]. The substitution of His-83 with Ala in Apn1 removes the ability of the mutant enzyme to cleave a substantially bent DNA duplex, as compared to WT Apn1 [23], due to the reduced number of Zn^{2+} ions in the active site of H83A Apn1.

While comparing H83A Apn1's AP endonuclease activity with that of the WT enzyme, we found that k_3 values for the mutant enzyme are one order of magnitude lower for ***F(2-aPu)*** and ***AP(2-aPu)*** substrates (see Table 2 and Ref. [23]). However, the affinity of H83A Apn1 to the DNA cleavage products was the same, as it was for WT Apn1. This indicates that His-83 and coordinated Zn^{2+} ions are not involved in product association–dissociation steps. Investigating H83A Apn1 interactions with ***(2-aPu)F*** and ***(2-aPu)AP*** duplexes revealed the inability of the mutant enzyme to effectively incise these substrates. Nevertheless, the

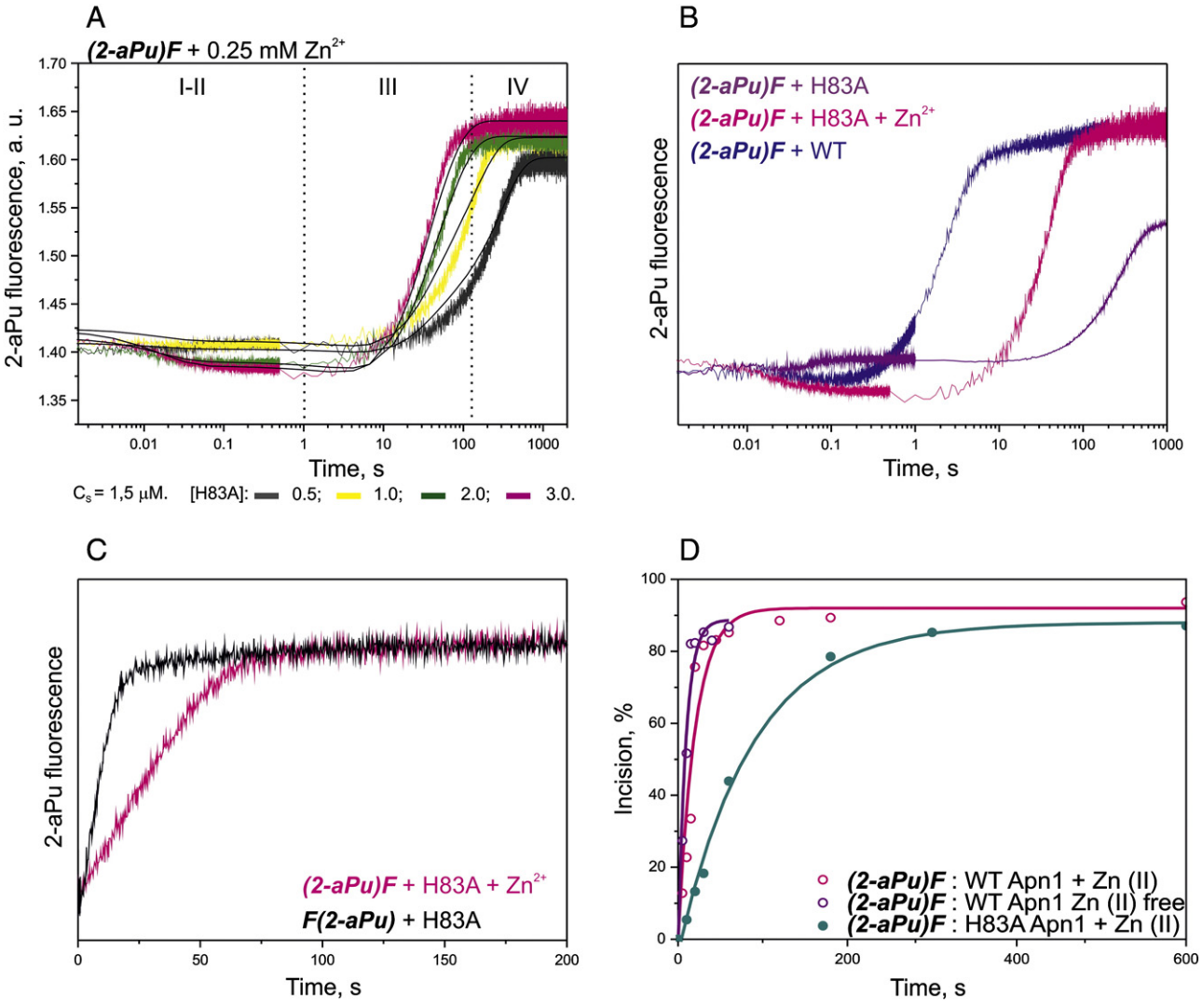

Fig. 11. Conformational dynamics of DNA duplexes during the interactions with WT and H83A mutant of Apn1. (A) ***(2-aPu)F*** duplex in the presence of Zn^{2+} interacting with H83A mutant. [DNA] = 1.5 μM, [enzyme] was varied 0.5, 1.0, 2.0, and 3.0 μM. [Zn^{2+}] = 0.25 mM. (B) Superposition of kinetic traces of H83A Apn1 and WT Apn1 interactions with ***(2-aPu)F*** duplex in the presence and in the absence of Zn^{2+}. [DNA] = 1.5 μM, [enzyme] = 3.0 μM, [Zn^{2+}] = 0.25 mM. (C) Superposition of kinetic traces of H83A Apn1 interactions with ***(2-aPu)F*** duplex in the presence of Zn^{2+} ions and ***F(2-aPu)*** duplex. [DNA] = 1.5 μM, [enzyme] = 3.0 μM, [Zn^{2+}] = 0.25 mM. (D) PAGE analysis of ***(2-aPu)F*** substrate incision by WT and H83A Apn1 in the presence and in the absence of Zn^{2+} ions. Pink—WT Apn1 interaction with ***(2-aPu)F*** substrate in the presence of 0.5 mM Zn^{2+}. Purple—WT Apn1 interaction with ***(2-aPu)F*** substrate in the absence of Zn^{2+}. Dark cyan—H83A Apn1 interaction with ***(2-aPu)F*** substrate in the presence of 0.25 mM Zn^{2+}.

affinity of the Apn1 mutant to these duplexes were comparable with effectively incised ***F(2-aPu)*** and ***AP(2-aPu)*** substrates. Fluorescence titration of H83A Apn1 with damaged ***(2-aPu)F*** and undamaged ***(2-aPu)G*** duplexes revealed different Trp fluorescence behaviors (see Supplementary Data, Fig. S5), probably indicating specific and non-specific binding, respectively. Comparing WT and H83A Apn1 association to damaged DNA identified differing affinities of the enzymes to the tested DNA duplexes (K_a^S). The most specific APE1 substrate was ***AP(2-aPu)***, which incised F-containing substrate slightly slower compared to the AP-containing one [23,25,50,56,58]. Interestingly, the affinities of WT and H83A Apn1 to potential ***(2-aPu)F*** incision products are also identical ($K_a^P = 2.5 \times 10^5\ M^{-1}$ in both cases). These results provide evidence that the outcome of His-83 substitution with Ala causes difficulties for both specific complex formation and catalytic reaction leading to a deceleration (in the case of ***F(2-aPu)*** and ***AP(2-aPu))*** or suppression (in the case of ***(2-aPu)F*** and ***(2-aPu)AP***) of the AP endonuclease reaction, without a beneficial influence on binding with DNA reaction products. Perhaps, the most intriguing and promising finding is the possibility to restore H83A Apn1's AP endonuclease activity in relation to ***(2-aPu)X*** duplexes by adding Zn^{2+} ions. This

Table 4
Rate and equilibrium constants for H83A Apn1 interaction with 5′-mismatched ***(2-aPu)F*** duplex in the presence of Zn^{2+} ions.

Shorthand	k_1 ($M^{-1}\ s^{-1}$)	k_{-1} (s^{-1})	K_1 (M^{-1})	k_2 (s^{-1})	k_{-2} (s^{-1})	K_2	k_3 (s^{-1})	K_a^S M^{-1}
(2-aPu)F + Zn^{2+}	(9.8 ± 0.1) × 10^5	58.9 ± 0.4	1.7 × 10^4	2.9 ± 0.04	0.036 ± 0.002	80.6	0.016 ± 0.001	1.2 × 10^6

supports the involvement of His-83 residue in Zn^{2+} coordination, and triggers the catalytic stage. Molecular dynamics of H83A Apn1–DNA complex confirmed our assumptions on the high significance of Apn1 His-83 residue in cleaving abasic sites during the base excision repair pathway. The data obtained shed light on the key aspects of the enzymatic mechanism, namely, the peculiar features of the conformational changes that DNA is undergoing during its interaction with the Apn1 mutant.

Transparency document

The Transparency document associated with this article can be found, in the version.

Acknowledgments

The work is supported by grants from the Program of the Russian Academy of Sciences "Molecular & Cell Biology" [6.11 to O.S.F.], the Russian Foundation for Basic Research [RFBR 13-04-00013 to O.S.F., 14-04-31201 to E.S.D., and 14-04-00806 to V.V.K.], the Russian Ministry of Education and Science [SS-1205.2014.4], the Fondation de France [2012 00029161 to A.A.I.].

Appendix A. Supplementary data

Supplementary data to this article can be found online at http://dx.doi.org/10.1016/j.bbagen.2015.03.001.

References

[1] J.M. Daley, C. Zakaria, D. Ramotar, The endonuclease IV family of apurinic/apyrimidinic endonucleases, Mutat. Res. 705 (2010) 217–227.
[2] L. Gros, M.K. Saparbaev, J. Laval, Enzymology of the repair of free radicals-induced DNA damage, Oncogene 21 (2002) 8905–8925.
[3] S. Boiteux, M. Guillet, Abasic sites in DNA: repair and biological consequences in *Saccharomyces cerevisiae*, DNA Repair (Amst) 3 (2004) 1–12.
[4] A.A. Ishchenko, G. Sanz, C.V. Privezentzev, A.V. Maksimenko, M. Saparbaev, Characterisation of new substrate specificities of *Escherichia coli* and *Saccharomyces cerevisiae* AP endonucleases, Nucleic Acids Res. 31 (2003) 6344–6353.
[5] A. Jilani, R. Vongsamphanh, A. Leduc, L. Gros, M. Saparbaev, D. Ramotar, Characterization of two independent amino acid substitutions that disrupt the DNA repair functions of the yeast Apn1, Biochemistry 42 (2003) 6436–6445.
[6] D. Ramotar, B. Demple, Functional expression of *Escherichia coli* endonuclease IV in apurinic endonuclease-deficient yeast, J. Biol. Chem. 271 (1996) 7368–7374.
[7] V.G. Korolev, Base excision repair: AP endonucleases and DNA polymerases, Genetika 41 (2005) 1301–1309.
[8] J.D. Levin, R. Shapiro, B. Demple, Metalloenzymes in DNA repair. *Escherichia coli* endonuclease IV and *Saccharomyces cerevisiae* Apn1, J. Biol. Chem. 266 (1991) 22893–22898.
[9] D. Ramotar, C. Kim, R. Lillis, B. Demple, Intracellular localization of the Apn1 DNA repair enzyme of *Saccharomyces cerevisiae*. Nuclear transport signals and biological role, J. Biol. Chem. 268 (1993) 20533–20539.
[10] K. Acevedo-Torres, S. Fonseca-Williams, S. Ayala-Torres, C.A. Torres-Ramos, Requirement of the *Saccharomyces cerevisiae* APN1 gene for the repair of mitochondrial DNA alkylation damage, Environ. Mol. Mutagen. 50 (2009) 317–327.
[11] L.L. Souza, I.R. Eduardo, M. Pádula, A.C. Leitão, Endonuclease IV and exonuclease III are involved in the repair and mutagenesis of DNA lesions induced by UVB in *Escherichia coli*, Mutagenesis 21 (2006) 125–130.
[12] S. Ljungquist, A new endonuclease from *Escherichia coli* acting at apurinic sites in DNA, J. Biol. Chem. 252 (1977) 2808–2814.
[13] R.P. Cunningham, S.M. Saporito, S.G. Spitzer, B. Weiss, Endonuclease IV (nfo) mutant of *Escherichia coli*, J. Bacteriol. 168 (1986) 1120–1127.
[14] S.C. Popoff, A.I. Spira, A.W. Johnson, B. Demple, Yeast structural gene (APN1) for the major apurinic endonuclease: homology to *Escherichia coli* endonuclease IV, Proc. Natl. Acad. Sci. U. S. A. 87 (1990) 4193–4197.
[15] A.A. Ishchenko, H. Ide, D. Ramotar, G. Nevinsky, M. Saparbaev, Alpha-anomeric deoxynucleotides, anoxic products of ionizing radiation, are substrates for the endonuclease IV-type AP endonucleases, Biochemistry 43 (2004) 15210–15216.
[16] R. Ho, L.I. Rachek, Y. Xu, M.R. Kelley, S.P. LeDoux, G.L. Wilson, Yeast apurinic/apyrimidinic endonuclease Apn1 protects mammalian neuronal cell line from oxidative stress, J. Neurochem. 102 (2007) 13–24.
[17] A.A. Ishchenko, X. Yang, D. Ramotar, M. Saparbaev, The 3'- > 5' exonuclease of Apn1 provides an alternative pathway to repair 7,8-dihydro-8-oxodeoxyguanosine in *Saccharomyces cerevisiae*, Mol. Cell. Biol. 25 (2005) 6380–6390.
[18] E.D. Garcin, D.J. Hosfield, S.A. Desai, B.J. Haas, M. Björas, R.P. Cunningham, J.A. Tainer, DNA apurinic-apyrimidinic site binding and excision by endonuclease IV, Nat. Struct. Mol. Biol. 15 (2008) 515–522.
[19] D. Ramotar, S.C. Popoff, E.B. Gralla, B. Demple, Cellular role of yeast Apn1 apurinic endonuclease/3'-diesterase: repair of oxidative and alkylation DNA damage and control of spontaneous mutation, Mol. Cell. Biol. 11 (1991) 4537–4544.
[20] L.P. Morris, N. Degtyareva, C. Sheppard, L. Heyburn, A.A. Ivanov, Y.W. Kow, P.W. Doetsch, *Saccharomyces cerevisiae* Apn1 mutation affecting stable protein expression mimics catalytic activity impairment: implications for assessing DNA repair capacity in humans, DNA Repair (Amst) 11 (2012) 753–765.
[21] X. Yang, J. Fan, A.A. Ishchenko, D. Patel, M.K. Saparbaev, D. Ramotar, Functional characterization of the *Caenorhabditis elegans* DNA repair enzyme APN-1, DNA Repair (Amst) 11 (2012) 811–822.
[22] D.J. Hosfield, Y. Guan, B.J. Haas, R.P. Cunningham, J.A. Tainer, Structure of the DNA repair enzyme endonuclease IV and its DNA complex: double-nucleotide flipping at abasic sites and three-metal-ion catalysis, Cell 98 (1999) 397–408.
[23] E.S. Dyakonova, V.V. Koval, A.A. Ishchenko, M.K. Saparbaev, R. Kaptein, O.S. Fedorova, Kinetic mechanism of the interaction of *Saccharomyces cerevisiae* AP-endonuclease 1 with DNA substrates, Biochemistry (Mosc) 77 (2012) 1162–1171.
[24] O.S. Fedorova, G.A. Nevinsky, V.V. Koval, A.A. Ishchenko, N.L. Vasilenko, K.T. Douglas, Stopped-flow kinetic studies of the interaction between *Escherichia coli* Fpg protein and DNA substrates, Biochemistry 41 (2002) 1520–1528.
[25] E.L. Rachofsky, E. Seibert, J.T. Stivers, R. Osman, J.B. Ross, Conformation and dynamics of abasic sites in DNA investigated by time-resolved fluorescence of 2-aminopurine, Biochemistry 40 (2001) 957–967.
[26] P. Kuzmic, Program DYNAFIT for the analysis of enzyme kinetic data: application to HIV proteinase, Anal. Biochem. 237 (1996) 260–273.
[27] N.A. Kuznetsov, Y.N. Vorobjev, L.N. Krasnoperov, O.S. Fedorova, Thermodynamics of the multi-stage DNA lesion recognition and repair by formamidopyrimidine-DNA glycosylase using pyrrolocytosine fluorescence–stopped-flow pre-steady-state kinetics, Nucleic Acids Res. 40 (2012) 7384–7392.
[28] N.A. Timofeyeva, V.V. Koval, D.G. Knorre, D.O. Zharkov, M.K. Saparbaev, A.A. Ishchenko, O.S. Fedorova, Conformational dynamics of human AP endonuclease in base excision and nucleotide incision repair pathways, J. Biomol. Struct. Dyn. 26 (2009) 637–652.
[29] L.Y. Kanazhevskaya, V.V. Koval, D.O. Zharkov, P.R. Strauss, O.S. Fedorova, Conformational transitions in human AP endonuclease 1 and its active site mutant during abasic site repair, Biochemistry 49 (2010) 6451–6461.
[30] K.R. Gee, Z.L. Zhou, W.J. Qian, R. Kennedy, Detection and imaging of zinc secretion from pancreatic beta-cells using a new fluorescent zinc indicator, J. Am. Chem. Soc. 124 (2002) 776–778.
[31] M.J. Devinney, I.J. Reynolds, K.E. Dineley, Simultaneous detection of intracellular free calcium and zinc using fura-2FF and FluoZin-3, Cell Calcium 37 (2005) 225–232.
[32] U. Consortium, Activities at the universal protein resource (UniProt), Nucleic Acids Res. 42 (2014) D191–D198.
[33] L.A. Kelley, M.J. Sternberg, Protein structure prediction on the Web: a case study using the Phyre server, Nat. Protoc. 4 (2009) 363–371.
[34] F. Sievers, A. Wilm, D. Dineen, T.J. Gibson, K. Karplus, W. Li, R. Lopez, H. McWilliam, M. Remmert, J. Söding, J.D. Thompson, D.G. Higgins, Fast, scalable generation of high-quality protein multiple sequence alignments using Clustal Omega, Mol. Syst. Biol. 7 (2011) 539.
[35] E.F. Pettersen, T.D. Goddard, C.C. Huang, G.S. Couch, D.M. Greenblatt, E.C. Meng, T.E. Ferrin, UCSF Chimera–a visualization system for exploratory research and analysis, J. Comput. Chem. 25 (2004) 1605–1612.
[36] M. Källberg, H. Wang, S. Wang, J. Peng, Z. Wang, H. Lu, J. Xu, Template-based protein structure modeling using the RaptorX web server, Nat. Protoc. 7 (2012) 1511–1522.
[37] H. Zheng, M.D. Chordia, D.R. Cooper, M. Chruszcz, P. Müller, G.M. Sheldrick, W. Minor, Validation of metal-binding sites in macromolecular structures with the CheckMyMetal web server, Nat. Protoc. 9 (2014) 156–170.
[38] M.M. Harding, Geometry of metal-ligand interactions in proteins, Acta Crystallogr. D Biol. Crystallogr. 57 (2001) 401–411.
[39] G. Kuppuraj, M. Dudev, C. Lim, Factors governing metal-ligand distances and coordination geometries of metal complexes, J. Phys. Chem. B 113 (2009) 2952–2960.
[40] L.Y. Kanazhevskaya, V.V. Koval, A.A. Lomzov, O.S. Fedorova, The role of Asn-212 in the catalytic mechanism of human endonuclease APE1: stopped-flow kinetic study of incision activity on a natural AP site and a tetrahydrofuran analogue, DNA Repair (Amst) 21C (2014) 43–54.
[41] R. Salomon-Ferrer, D.A. Case, R.C. Walker, An overview of the Amber biomolecular simulation package, WIREs Comput. Mol. Sci. 3 (2013) 198–210.
[42] D.A. Case, T.A. Darden, T.E. Cheatham III, C.L. Simmerling, J. Wang, R.E. Duke, R. Luo, R.C. Walker, W. Zhang, K.M. Merz, B. Roberts, S. Hayik, A. Roitberg, G. Seabra, J. Swails, A.W. Götz, I. Kolossváry, K.F. Wong, F. Paesani, J. Vanicek, R.M. Wolf, J. Liu, X. Wu, S.R. Brozell, T. Steinbrecher, H. Gohlke, Q. Cai, X. Ye, J. Wang, M.-J. Hsieh, G. Cui, D.R. Roe, D.H. Mathews, M.G. Seetin, R. Salomon-Ferrer, C. Sagui, V. Babin, T. Luchko, S. Gusarov, A. Kovalenko, P.A. Kollman, AMBER 12, University of California, San Francisco, 2012.
[43] D.A. Case, AMBER parameter database, University of Manchester, The database is maintained by Richard Bryce.
[44] R.H. Stote, M. Karplus, Zinc binding in proteins and solution: a simple but accurate nonbonded representation, Proteins 23 (1995) 12–31.
[45] A.W. Götz, M.J. Williamson, D. Xu, D. Poole, S. Le Grand, R.C. Walker, Routine microsecond molecular dynamics simulations with AMBER on GPUs. 1. Generalized born, J. Chem. Theory Comput. 8 (2012) 1542–1555.
[46] R. Salomon-Ferrer, A.W. Götz, D. Poole, S. Le Grand, R.C. Walker, Routine microsecond molecular dynamics simulations with AMBER on GPUs. 2. Explicit solvent particle mesh Ewald, J. Chem. Theory Comput. 9 (2013) 3878–3888.

[47] V. Hornak, R. Abel, A. Okur, B. Strockbine, A. Roitberg, C. Simmerling, Comparison of multiple Amber force fields and development of improved protein backbone parameters, Proteins 65 (2006) 712–725.
[48] A. Pérez, I. Marchán, D. Svozil, J. Sponer, T.E. Cheatham, C.A. Laughton, M. Orozco, Refinement of the AMBER force field for nucleic acids: improving the description of alpha/gamma conformers, Biophys. J. 92 (2007) 3817–3829.
[49] The PyMOL Molecular Graphics System, 1.6.0.0 Schrödinger, LLC, 2002.
[50] L.Y. Kanazhevskaya, V.V. Koval, Y.N. Vorobjev, O.S. Fedorova, Conformational dynamics of abasic DNA upon interactions with AP endonuclease 1 revealed by stopped-flow fluorescence analysis, Biochemistry 51 (2012) 1306–1321.
[51] V. Purohit, N.D. Grindley, C.M. Joyce, Use of 2-aminopurine fluorescence to examine conformational changes during nucleotide incorporation by DNA polymerase I (Klenow fragment), Biochemistry 42 (2003) 10200–10211.
[52] C.A. Dunlap, M.D. Tsai, Use of 2-aminopurine and tryptophan fluorescence as probes in kinetic analyses of DNA polymerase beta, Biochemistry 41 (2002) 11226–11235.
[53] G. Tamulaitis, M. Zaremba, R.H. Szczepanowski, M. Bochtler, V. Siksnys, Nucleotide flipping by restriction enzymes analyzed by 2-aminopurine steady-state fluorescence, Nucleic Acids Res. 35 (2007) 4792–4799.
[54] S.M. Law, R. Eritja, M.F. Goodman, K.J. Breslauer, Spectroscopic and calorimetric characterizations of DNA duplexes containing 2-aminopurine, Biochemistry 35 (1996) 12329–12337.
[55] D.M. Wilson, M. Takeshita, A.P. Grollman, B. Demple, Incision activity of human apurinic endonuclease (Ape) at abasic site analogs in DNA, J. Biol. Chem. 270 (1995) 16002–16007.
[56] N.A. Timofeyeva, V.V. Koval, A.A. Ishchenko, M.K. Saparbaev, O.S. Fedorova, Lys98 substitution in human AP endonuclease 1 affects the kinetic mechanism of enzyme action in base excision and nucleotide incision repair pathways, PLoS One 6 (2011) e24063.
[57] B. Demple, L. Harrison, D.M. Wilson, R.A. Bennett, T. Takagi, A.G. Ascione, Regulation of eukaryotic abasic endonucleases and their role in genetic stability, Environ. Health Perspect. 105 (Suppl. 4) (1997) 931–934.
[58] K.M. Schermerhorn, S. Delaney, Transient-state kinetics of apurinic/apyrimidinic (AP) endonuclease 1 acting on an authentic AP site and commonly used substrate analogs: the effect of diverse metal ions and base mismatches, Biochemistry 52 (2013) 7669–7677.
[59] R.L. Maher, L.B. Bloom, Pre-steady-state kinetic characterization of the AP endonuclease activity of human AP endonuclease 1, J. Biol. Chem. 282 (2007) 30577–30585.
[60] A. Sassa, W.A. Beard, R. Prasad, S.H. Wilson, DNA sequence context effects on the glycosylase activity of human 8-oxoguanine DNA glycosylase, J. Biol. Chem. 287 (2012) 36702–36710.
[61] D. Whitford, Proteins: structure and function, John Wiley & Sons, Ltd., Chichester, England, 2005.
[62] A. Dallmann, L. Dehmel, T. Peters, C. Mügge, C. Griesinger, J. Tuma, N.P. Ernsting, 2-Aminopurine incorporation perturbs the dynamics and structure of DNA, Angew. Chem. Int. Ed. Engl. 49 (2010) 5989–5992.
[63] A.A. Ishchenko, E. Deprez, A. Maksimenko, J.C. Brochon, P. Tauc, M.K. Saparbaev, Uncoupling of the base excision and nucleotide incision repair pathways reveals their respective biological roles, Proc. Natl. Acad. Sci. U. S. A. 103 (2006) 2564–2569.
[64] C.D. Mol, D.J. Hosfield, J.A. Tainer, Abasic site recognition by two apurinic/apyrimidinic endonuclease families in DNA base excision repair: the 3′ ends justify the means, Mutat. Res. 460 (2000) 211–229.